CDKN2A/p16INK4a suppresses hepatic fatty acid oxidation through the AMPKα2-SIRT1-PPARα signaling pathway

Yann Deleye, Alexia Karen Cotte, Sarah Anissa Hannou, Nathalie Hennuyer, Lucie Bernard, Bruno Derudas, Sandrine Caron, Vanessa Legry, Emmanuelle Vallez, Emilie Dorchies, et al.

CDKN2A/p16INK4a suppresses hepatic fatty acid oxidation through the AMPKα2-SIRT1-PPARα signaling pathway.

Yann Deleye[1,5,6], Alexia Karen Cotte[1,5], Sarah Anissa Hannou[1,6], Nathalie Hennuyer[1], Lucie Bernard[1] Bruno Derudas[1], Sandrine Caron[1], Vanessa Legry[1], Emmanuelle Vallez[1], Emilie Dorchies[1], Nathalie Martin[2], Steve Lancel[1], Jean Sébastien Annicotte[3], Kadiombo Bantubungi[1], Albin Pourtier[2], Violeta Raverdy[4], François Pattou[4], Philippe Lefebvre[1], Corinne Abbadie[2], Bart Staels[1,7], Joel T. Haas[1,7], Réjane Paumelle[1,7*]

From the [1] Univ. Lille, Inserm, CHU Lille, Institut Pasteur de Lille, U1011- EGID, F-59000 Lille, France; [2] Univ. Lille, CNRS, Institut Pasteur de Lille, UMR 8161 – M3T – Mechanisms of Tumorigenesis and Target Therapies, F-59000 Lille, France; [3] Univ. Lille, CNRS, CHU Lille, Institut Pasteur de Lille, UMR 8199 – EGID, F-59000 Lille, France; [4] Univ. Lille, Inserm, CHU Lille, UMR 1190 – EGID, F-59000 Lille, France

Running title: p16INK4a controls hepatic fatty acid oxidation

[5] These authors contributed equally
[6] Present address: Duke Molecular Physiology Institute, Duke University Medical Center, 300 North Duke Street, Durham, NC 27701, USA
[7] These authors jointly supervised the study
* To whom correspondence should be addressed: Réjane Paumelle. Inserm U1011, Institut Pasteur de Lille, 1 rue du Professeur Calmette, BP245, Lille 59019, France, Tel: +33 3 20 97 42 09, Fax: +33 3 20 97 42 01, E-mail: rejane.lestrelin@univ-lille.fr

Keywords: CDKN2A, PPARα, liver, lipid metabolism, fatty acid oxidation, AMPKα, steatosis

ABSTRACT

In addition to their well-known role in the control of cellular proliferation and cancer, cell cycle regulators are increasingly identified as important metabolic modulators. Several GWAS have identified SNPs near *CDKN2A*, the locus encoding for p16INK4a (p16), associated with elevated risk for cardiovascular diseases and type-2 diabetes development, two pathologies associated with impaired hepatic lipid metabolism. Although p16 was recently shown to control hepatic glucose homeostasis, it is unknown whether p16 also controls hepatic lipid metabolism. Using a combination of *in vivo* and *in vitro* approaches, we found that p16 modulates fasting-induced hepatic fatty acid oxidation (FAO) and lipid droplet accumulation. In primary hepatocytes, p16-deficiency was associated with elevated expression of genes involved in fatty acid catabolism. These transcriptional changes led to increased FAO and were associated with enhanced activation of PPARα through a mechanism requiring the catalytic AMPKα2 subunit and SIRT1, two known activators of PPARα. By contrast, *p16* overexpression was associated with triglyceride accumulation and increased lipid droplet numbers *in vitro*, and decreased ketogenesis and hepatic mitochondrial activity *in vivo*. Finally, gene expression analysis of liver samples from obese patients revealed a negative correlation between *CDKN2A* expression and *PPARA* and its target genes. Our findings demonstrate that p16 represses hepatic lipid catabolism during fasting and may thus participate in the preservation of metabolic flexibility.

INTRODUCTION

Cell cycle regulators have been extensively studied in the context of proliferation, cancer development and aging (1). Progression through the cell cycle requires specific metabolic programs for synthesis of cellular building blocks or ATP production (2). Interestingly, recent work has shown that several cell cycle regulators also modulate metabolism in non-proliferative cells, suggesting new physiological functions of this large family of proteins (3).

P16INK4a (p16) is a Cyclin-Dependent-Kinase Inhibitor that blocks activation of E2F transcription factors via inhibition of CDK4/6 (4). Interestingly, several GWAS have identified SNPs near *CDKN2A*, the locus encoding for p16, as associated with elevated risk for cardiovascular

disease (CVD) and type-2 diabetes (T2D) development (5). In line, we recently reported that p16-deficient mice display elevated hepatic gluconeogenesis during fasting due to activation of a cascade involving CDK4, PKA, CREB, and PGC1α in hepatocytes, suggesting an important role for p16 in metabolic control (6). Interestingly, other cell cycle regulators in the CDK4/Cyclin D - E2F1 pathway, downstream of p16, have also been implicated in the control of hepatic lipid metabolism (7,8). In addition, impaired hepatic lipid metabolism (e.g. as seen during aging or exposure to high fat diet feeding) is associated with increased hepatic expression of p16 (9,10). However, whether p16 directly regulates hepatic lipid homeostasis remains unknown.

The AMP-Activated Protein Kinase (AMPK) is an important regulator of hepatic lipid homeostasis. During prolonged fasting, AMPK senses cellular energetic deficit and activates FAO to reestablish normal energy balance (11). AMPK is a heterotrimeric complex composed of one catalytic subunit α and two regulatory subunits β and γ, each of which have several different isoforms. There are two catalytic subunit isoforms, AMPKα1 (PRKAA1) and AMPKα2 (PRKAA2), and their phosphorylation at T172 is critical for AMPK activation. The tissue expression of these two isoforms is different, however, whether there are specific roles for each isoform remains unresolved. Interestingly, CDK4 phosphorylates AMPKα2, and not AMPKα1, at several sites (other than T172) thereby suppressing AMPK activity and FAO (12). Moreover, other cell cycle regulators such as Cyclin D1, a CDK4 partner (13), inhibit the activity of PPARα, a master regulator of lipid metabolism gene expression and downstream effector of AMPK activation. Overall, these studies highlight the close interplay between cell cycle and energy balance regulators.

In this study, we assessed the effects of hepatic p16 expression on fasting lipid metabolism, and found that modulation of p16 expression regulates hepatic FAO, mitochondrial function and ketogenesis. P16-deficiency leads to activation of a cascade involving AMPKα2, SIRT1 and PPARα, which drives enhanced expression of lipid catabolism genes. Interestingly, we found these effects of p16-deficiency to be independent of changes in CDK4 activity. Moreover, adenovirus-mediated overexpression of p16 led to accumulation of LD *in vitro,* and decreased hepatic mitochondrial activity and ketogenesis *in vivo*. Our findings highlight a new role for p16 in the hepatic response to fasting and uncover a novel mechanism by which p16 may contribute to the development of metabolic diseases via modulation of hepatic mitochondrial function.

RESULTS

P16-deficiency increases fatty acid catabolic gene expression in hepatocytes

To determine whether p16-deficiency affects hepatic lipid metabolism, we performed transcriptomic profiling of primary hepatocytes isolated from $p16^{+/+}$ and $p16^{-/-}$ mice cultured under conditions mimicking fasting (as described in the methods section). There were 3289 differentially expressed genes between $p16^{+/+}$ and $p16^{-/-}$ cells (FDR < 0.2). Gene Ontology terms enrichment analysis revealed that several metabolic pathways are significantly affected by p16-deficiency, including oxidation-reduction, alpha-amino acid metabolism, and xenobiotic metabolism (**Figure 1A**), suggesting that p16 regulates mitochondrial and peroxisomal functions. As expected, principle component analysis (PCA) of the 3289 differentially expressed genes identified a clear separation based on p16 genotype (**Figure 1B**). Interestingly, the loadings for several genes involved in fatty acid oxidation (FAO) and ketogenesis (e.g. *Cpt1a, Ehhadh, Hmgcs2, Bdh1*) were highly correlated with PC1 (**Figure 1B)**, indicating that their expression pattern contributes strongly to the difference between the $p16^{+/+}$ and $p16^{-/-}$ transcriptomes. We then specifically investigated metabolic pathways associated with fatty acid (FA) mobilization, storage and utilization (**Figure 1C**). Interestingly, p16-deficiency was associated with marked changes in these pathways, including activation of both mitochondrial and peroxisomal catabolic pathways (e.g. *Ehhadh*, *Cpt1a*, *Hmgcs2* and *Bdh1,* **Figure S1A**).

Because primary hepatocytes from p16-deficient mice could be affected by an altered developmental program due to p16-deficiency, we next tested whether acute modulation of p16 expression was sufficient to induce similar changes in gene expression *in vitro*. In murine AML12 cells (**Figure 1D**) and immortalized human hepatocytes (IHH, **Figure 1E**), siRNA

mediated reduction of p16 led to a strong increase in several genes identified in the transcriptomic analysis, including *HMGCS2*, *CPT1A*, and *EHHADH*. Furthermore, adenovirus-mediated p16-overexpression in HepG2 cells resulted in reduced expression of these same genes (**Figure 1F**). Taken together, these results indicate that p16-deficiency in hepatocytes leads to the induction of a transcriptional program indicative of increased fatty acid utilization.

P16 controls mitochondrial fatty acid oxidation and lipid droplet formation in hepatocytes

We next sought to investigate whether activation of lipid metabolism gene expression as a result of p16-deficiency is reflected by corresponding functional changes in hepatocyte lipid metabolism and mitochondrial function. Measurement of β-oxidation with ^{14}C-labeled oleic acid in $p16^{+/+}$ and $p16^{-/-}$ primary hepatocytes revealed that formation of $^{14}CO_2$ (complete oxidation, **Figure 2A**) was increased in $p16^{-/-}$ compared to $p16^{+/+}$ cells, and associated with a tendency towards higher ^{14}C-acid soluble metabolites, mostly ketone bodies in hepatocytes (incomplete oxidation, **Figure 2B**). To test whether hepatic mitochondrial activity and ketone body production are also modulated by p16 *in vivo*, we first assessed fasting blood β-hydroxybutyrate (βOHB) levels, which account for ~ 75% of circulating ketone bodies in mice (14). Unexpectedly, βOHB concentration did not differ between $p16^{+/+}$ and $p16^{-/-}$ mice after overnight fasting (**Figure 2C**). However, acute injection of overnight fasted mice with octanoate, a medium chain fatty acid shown to specifically activate hepatic ketogenesis (15), resulted in a statistically significant augmentation in blood βOHB levels in p16-/- mice within 60 minutes. Moreover, the area under the curve of βOHB was also higher in $p16^{-/-}$ mice compared to $p16^{+/+}$ littermate controls (**Figure 2D**). Finally, we tested whether liver-specific p16 overexpression by adenovirus is sufficient to decrease hepatic mitochondrial function in C57BL6/J mice. Hepatic p16 overexpression (**Figure S2A**) resulted in a significant decrease in fasting blood βOHB levels (**Figure 2E**) and hepatic mitochondrial respiratory control ratio (RCR) measured in the presence of palmitoyl-carnitine (**Figure 2F)** when compared to GFP-overexpressing controls. Importantly, these changes were independent of differences in body weight (**Figure S2B**) and plasma free fatty acids (**Figure S2C**), the main substrate for ketone body synthesis.

To test which mitochondrial processes were most affected by p16-deficiency, oxygen consumption measurements using the Seahorse Extracellular Flux Analyzer were performed. Interestingly, p16 siRNA transfected IHH cells displayed increased maximal respiration capacity compared to control siRNA transfected cells (**Figure 2G** and **S3A**). Finally, we assessed the effect of p16-knockdown on intracellular triglyceride and lipid droplet (LD) accumulation by BODIPY staining. P16-knockdown resulted in a significant decrease in LD number per cell (**Figure 2H-I**), which was associated with decreased expression of perilipin 2 (*PLIN2*, **Figure 2J**), an LD-associated protein whose expression correlates with intracellular lipid storage. In line with the decreased mitochondrial activity observed *in vivo* (**Figure 2E-F**), p16 overexpression in HepG2 cells resulted in a strong increase (>20-fold) in LD per cell compared to control infected cells (**Figure 2K-L**), and associated with increased *PLIN2* expression (**Figure 2M**). These results indicate that p16 overexpression leads to accumulation of intracellular LD accompanied by reduced mitochondrial FAO.

p16 expression modulates HMGCS2 expression independently of CDK4

Thus far, we have demonstrated that modulation of p16 expression leads to changes in fatty acid metabolism in both non-proliferative primary hepatocytes and proliferating hepatocyte cell lines, indicating that p16's action on this pathway may be independent of its role in cell cycle regulation. The canonical function of p16 is to block the G0 to S phase transition via inhibition of CDK4-mediated phosphorylation of Rb protein (4). Consequently, we analyzed whether the p16-dependent changes in mitochondrial activity were associated with altered cell cycle progression. To do so, we first analyzed changes in CDK4 protein levels and Rb phosphorylation in p16-silenced IHH cells (**Figure 3A**). As expected (16), both CDK4 expression and Rb phosphorylation were reduced within 1-4h of shifting cells to conditions mimicking fasting (low glucose, no insulin, supplemented with forskolin). Interestingly, p16-silencing did not affect total CDK4 nor Rb phosphorylation under these conditions (**Figure 3A**). Moreover, p16-silencing in these cells did not modify cell cycle progression as measured by propidium iodide

staining (**Figure 3B**). Finally, we assessed whether CDK4 activation was also required for the regulation of *HMGCS2* gene expression upon p16-deletion. Pharmacological CDK4 inhibition by PD0332991 (Palbociclib, PD033) (**Figure 3C**) or CDK4-silencing by siRNA (**Figure 3D and S4A**) did not affect the siRNA-p16-mediated increase in *HMGCS2* expression.

Because p16 overexpression is associated with a senescent phenotype and senescence increases LD accumulation in hepatocytes (9), we assessed several parameters of senescence in ad-p16 overexpressing HepG2 cells (**Figure 2K-M**). A kinetic study of adenovirus-mediated p16 overexpression in HepG2 cells showed no differences in p21 mRNA expression, a marker of senescence, between ad-p16 and ad-Control cells at 24h and 48h post-infection. However, an increase of p21 transcript levels was observed in ad-p16-infected HepG2 cells after 72h **(Figure S4B-C).** Interestingly, the modest increase in p21 mRNA observed at the 72h time point was not associated with modulation of cell cycle progression nor with an increase of SA-β-Galactosidase activity, as measured by C12FDG staining, suggesting that p16 overexpression may not fully induce senescence in this time-frame **(Figure S4D-E)**. Conversely, BODIPY staining showed that ad-p16 infected HepG2 cells present significantly more lipid droplets per cell as early as 24h post-infection and this is maintained up to 72h **(Figure S4F-G)**. This effect is associated with a gradual and significant increase of *PLIN2* mRNA expression at 48h and 72h and a significant decrease of *HMGCS2* mRNA expression at 72h post-infection **(Figure S4H-I)**. In addition, adenovirus-mediated p16 overexpression in the liver was associated with decreased p21 mRNA expression and no changes in hepatic β-Galactosidase activity (**Figure S4J-K**). Taken together, these data suggest that p16 overexpression in hepatocytes may impact lipid metabolism prior to a possible induction of cellular senescence.

These results indicate that the effects of p16 on hepatocyte mitochondrial activity are unlikely to be mediated by modification of cell cycle progression and occur independently of CDK4 activity.

P16 protein expression is modulated by nutritional changes in IHH cells

We then wondered if suppression of p16 expression was a physiological mechanism occurring during fasting. *P16* mRNA expression was assessed in the liver of mice fasted overnight and refed for 6h or 24h (**Figure 4A**) or in mouse primary hepatocytes (**Figure 4B**) and IHH cells (**Figure 4C**) incubating in media mimicking fed or fasted conditions. None of these nutritional changes altered the expression of p16 at the mRNA level. Interestingly, p16 protein levels were increased in IHH cells in the refeeding experiment (**Figure 4D-E**), suggesting that p16 is regulated post-translationally. A recent report demonstrated that p16 is degraded by autophagy (17). Accordingly, rapamycin treatment for 8h in IHH cells led to a strong decrease of p16 protein (**Figure 4F**), suggesting that autophagy-mediated p16 degradation likely links nutritional status to p16 activity in hepatocytes.

P16-silencing activates the AMPKα2-SIRT1 pathway

To further dissect the mechanism of gene regulation by p16, we focused on *HMGCS2* expression. We first assessed whether p16 may inhibit AMPK, an important regulator of hepatic FAO and mitochondrial function, to drive changes in gene expression. Interestingly, p16-silencing in IHH cells resulted in increased AMPK phosphorylation at T172 (**Figure 5A**), a marker of AMPK activation. Moreover, siRNA knockdown of the AMPKα2 catalytic subunit (si*PRKAA2*) (**Figure 5B-C, and S5A**) abrogated the p16-dependent increase in *HMGCS2* expression, while knockdown of the AMPKα1 (si*PRKAA1*) catalytic subunit had no effect (**Figure S5B-D**). Interestingly, we found that knockdown of *AMPKα1* increased *HMGCS2* expression and decreased *PLIN2* expression in IHH cells (**Figure S5H**), while knockdown of the AMPKα2 increased *PLIN2* expression (**Figure S5I**), mimicking the effects observed after knockdown or overexpression of p16, respectively. P16-silencing in IHH cells also increased mRNA and protein expression/nuclear localization of AMPKα2, but not AMPKα1 (**Figure 5B-D and S5C-G**), suggesting that p16-silencing may also increase AMPK activity specifically through activation of the AMPKα2 catalytic subunit. In line, reduced total AMPK and AMPK phosphorylation at T172 were

observed in livers of overnight fasted mice overexpressing p16 (**Figure 5E**). Finally, p16-knockdown in IHH cells was associated with increased mitochondrial ROS, an activating signal for AMPK (18), but not total intracellular ROS (**Figure 5F-G**).

Because AMPK activation increases the NAD^+/NADH ratio leading to SIRT1 activation (19), the role of SIRT1 in the p16-mediated regulation of *HMGCS2* gene expression was also assessed. Treatment of IHH cells with EX527 (**Figure 5H, S5J**), a pharmacological SIRT1 inhibitor, or siRNA-mediated silencing of *SIRT1* (**Figure 5I-J, S5K**) abrogated the increase of *HMGCS2* gene expression upon p16-silencing. Altogether, these data suggest that p16-silencing increases *HMGCS2* expression and mitochondrial activity via an AMPKα2 and SIRT1-dependent signaling pathway.

P16 regulates fatty acid catabolism via activation of PPARα in hepatocytes

As PPARα is a master regulator of fasting-induced ketogenesis and a key effector of AMPK activation (20), we next assessed the effects of p16-silencing on PPARα activation *in vitro*. PPARα activation using the specific agonist GW7647 increased *HMGCS2* mRNA expression in primary murine hepatocytes, AML12, IHH and HepG2 cells and p16-silencing potentiated this induction (**Figure 6A-C, S6A-D**) in all models. Conversely, PPARα-knockdown partially blocked the induction of *HMGCS2* mRNA upon p16-silencing in AML12 and IHH cells (**Figure 6D-E, S6E-H**). To assess whether p16 may regulate FAO and mitochondrial function in human liver, expression of *CDKN2A*, *PPARA* and *HMGCS2* was measured in liver biopsies from a cohort of obese patients (n=910 patients) (21). Interestingly, *CDKN2A* gene expression negatively correlated with *HMGCS2* (Pearson $r = -0.49$; $p < 1 \times 10^{-16}$, **Figure 6F**) and *PPARA* ($r = -0.68$; $p < 1 \times 10^{-16}$, **Figure 6G**) gene expression, suggesting that p16 may also regulate hepatic ketogenesis in humans.

DISCUSSION

In the present study, we describe a novel function of the cell cycle inhibitor p16 as a regulator of hepatic fatty acid metabolism. P16-deletion in both murine and human hepatocytes enhanced fatty acid oxidation and ketogenesis by a mechanism involving activation of AMPKα2, SIRT1 and, consequently, PPARα. Moreover, our data indicate that regulation of these target genes by p16 is independent of its action on CDK4 and independent of alterations in cell cycle progression.

Cell cycle-independent regulation of metabolism is increasingly becoming an established function of many cell cycle regulators. The CDK4-E2F1 pathway was shown to increase hepatic lipogenesis and decrease FAO in non-proliferating cells under feeding conditions (7,8), thus contributing to steatosis and NAFLD development. In contrast, Cyclin D1, a CDK4 partner, was demonstrated to inhibit hepatic lipogenesis through repression of ChREBP, HNF4 (22) and PPARγ (23). More recently, Cyclin D1 was found to inhibit PPARα transcriptional activity in a CDK4-independent manner (13), highlighting the complexity of metabolic regulation by cell cycle regulators. Our data indicate that p16 inhibits fasting-induced FAO through PPARα modulation independently of CDK4 inhibition, suggesting that p16 and CDK4 may exert opposing actions on FA metabolism, perhaps depending on the nutritional context. Further studies are necessary to better understand the interplay of p16 and CDK4 on hepatic metabolic functions.

Our results show that p16 acts via AMPK and SIRT1 to modulate PPARα transcriptional activity in hepatocytes. AMPK and SIRT1 are important nutrient sensors regulating FAO during fasting. SIRT1 deacetylates PGC1α, thereby increasing its association with PPARα and subsequent transcriptional activity (24). Previous studies suggest that the AMPKα2 catalytic isoform controls the balance between lipogenesis and FAO in the liver (25). More recently, AMPKα2 was also shown to be required for efficient FAO in MEFs (12). Several studies have shown that the AMPKα2 subunit could be nuclear localized (26,27), and previous work from our group has shown that AMPK is recruited to chromatin and participates in transcriptional regulation with glucocorticoid receptor and PPARα (28). In the present study, we show that p16-silencing is associated with increased AMPK T172 phosphorylation and a specific increase in the mRNA and protein expression of the AMPKα2 (but not α1). Furthermore, only knockdown of AMPKα2 was sufficient to reverse the effects of p16-silencing on *HMGCS2* gene expression. In line, adenovirus-mediated p16 overexpression in the liver *in vivo* decreases FAO

and AMPK expression and phosphorylation. Together, these results suggest that p16 could specifically activate the AMPKα2 isoform to modulate PPARα transcriptional activity.

The mechanism by which AMPKα2 activity is regulated in hepatocytes is not fully understood. AMPK is an energetic sensor that is also highly sensitive to the cellular redox state. Indeed, AMPK can be activated by ROS-induced ATP depletion (18) and various mechanisms of direct ROS interaction (29,30). Increased mtROS production, as observed upon p16-knockdown, could thus explain increased AMPK activity (**Figure 5G**). However, further studies are required to better characterize the signaling cascade leading to a specific activation of AMPKα2 in p16-deficient hepatocytes.

We observed that p16 protein level is increased in IHH cells during refeeding conditions, without modulation of p16 mRNA expression by fasting. In line, p16 protein was recently demonstrated to be degraded by autophagy (17), a process induced by fasting and inhibited by refeeding (31,32). Moreover, partial deletion of ATG5 in mice, resulting in inhibition of autophagy, increased p16 protein levels in the liver (33). We propose that p16 protein degradation during fasting, likely via an autophagy-dependent mechanism, could participate in the physiological activation of FAO by PPARα in hepatocytes.

In line with our previous study showing that p16-deficiency enhances gluconeogenesis through the CDK4-PKA-CREB pathway (6), the increased PPARα activity upon p16-deficiency could also contribute to this increase via regulation of the expression of several genes involved in the conversion of glycerol to glucose (34) or modulation of substrate utilization. Indeed, both pyruvate (via expression of *Pdk4)* (35) and glycerol (36) metabolism are sensitive to PPARα modulation.

Finally, we observed that while overexpression of p16 in HepG2 cells increases lipid accumulation, p16 impacts neither the cell cycle nor senescence in hepatocytes in the conditions studied. In line, adenovirus-mediated overexpression of p16 in the mice livers led to a decrease of circulating ketone bodies and mitochondrial activity in the presence of palmitoyl-carnitine without induction of senescence. Aging and senescence are associated with decreased fatty acid oxidation resulting in increased hepatic fat accumulation (9). While p16 expression is a widely used marker of senescence, recent evidence suggests that a senescence-associated increase in liver p16 expression may not be related to its expression in hepatocytes (37,38). It is also possible that increased p16 may impact these metabolic pathways prior to the onset of outright senescence in a chronic setting.

Overall, our results provide further evidence that p16 plays an important role in the regulation of hepatic glucose and lipid metabolism and again support the genetic link between p16/CDKN2A and metabolic disorders such as T2D and CVD. Lowering p16 expression may help to restore hepatic FAO and lipid homeostasis by activating the AMPKα2-SIRT1-PPARα signaling pathway.

METHODS

Genetic terminology: *CDKN2A* vs *P16*

The use of *CDKN2A* in the manuscript refers to the entire *CDKN2A* locus (*P16* and *P14ARF* in human or *P19arf* in mouse), when analysis of *P16* mRNA expression alone or its modulation was not possible (Human liver transcriptomic data or siRNA-mediated knockdown of p16 in the murine AML12 cell line). Conversely, when using the terminology *P16*, this means that analysis of *P16* mRNA expression alone or its modulation was technically possible (siRNA in human cell lines, adenovirus-mediated overexpression of *P16* or measure of *P16* mRNA expression by QPCR).

Mouse model and diets

$p16^{-/-}$ and littermate control ($p16^{+/+}$) mice on a C57Bl6/J background (provided by P. Krimpenfort and backcrossed more than 8 generations) were housed under SPF conditions (22 ± 2°C) in conventional cages with free access to water and food unless indicated otherwise. Experimental procedures were conducted with the approval of the ethics committee for animal experimentation of the Nord Pas-de-Calais region (APAFIS#12317-2015121612289958 V15).

Ketogenesis assay in vivo. Following an overnight fast, 12-week-old $p16^{+/+}$ (n=9) and $p16^{-/-}$ (n=9) male mice were injected with 250 mM sodium octanoate and β-hydroxybutyrate was measured with a ketometer and β-ketone test strips (Abbott Diabetes Care, Freestyle Optium

Neo) before the injection and every 30 min following the injection.

Adenoviral-mediated overexpression of p16. 16-week-old male mice were injected via the tail vein with a solution containing $1x10^8$ genome copies of ad-GFP (n=10) or ad-p16 (n=11). Four days after adenovirus injections, mice were fasted overnight, plasma β-hydroxybutyrate was measured as described above, and livers were harvested for mitochondrial function analysis.

Primary hepatocyte isolation, culture and treatments

Primary hepatocytes were isolated from 12-week-old male mice using the two-step collagenase perfusion method, essentially as described previously (6). Following isolation, cells were seeded on collagen-coated plates in Williams E media (Life Technologies) supplemented with 0.1% BSA, 2 mM glutamine, 100 nM bovine insulin, 100 nM dexamethasone, and penicillin and streptomycin. The following morning, cells were washed with PBS and incubated in DMEM, 1mM glucose, supplemented with 0.1% BSA and antibiotics for 8h, described as fasting conditions.

Microarray analysis

Mouse primary hepatocytes transcriptomics. Analysis was performed using Mouse Gene 2.0ST arrays (Affymetrix). Array data processing was performed using Bioconductor in the R-environment (r-project.org). Gene expression changes were calculated after signal normalization using robust multichip averaging (RMA) in the *oligo* package (39). Differential gene expression was assessed using the *limma* package (40) with a threshold of 5% false discovery rate (FDR). Gene Ontology (GO) terms enrichment of selected clusters was performed using the *clusterProfiler* package (41,42).

Human liver transcriptomics. Liver biopsies were obtained from morbidly obese patients during abdominal surgery. Patients underwent a full clinical workup to assess metabolic characteristics and surgical risks. All experimental procedures abide by the Declaration of Helsinki Principles and written informed consent was obtained from each participant as part of the ABOS protocol (ID: NCT01129297). The protocol was also reviewed and approved by the Lille University Hospital ethical committee. RNA quality was assessed using the Agilent Bioanalyzer and only samples with RIN > 5 were included for analysis. Transcriptomic analysis of human liver biopsies was performed using Affymetrix HTA 2.0 arrays (21). Array pre-processing and gene expression analysis were performed as described for murine arrays. Basic clinical characteristics of the patient population are provided in Supplemental Table S1.

Cell culture, siRNA and adenovirus experiments

Alpha Mouse Liver 12 (AML12), Human Immortalized Hepatocytes (IHH) and Human Hepatoma cell line HepG2 were maintained as described in the method details in a humidified incubator at 37°C under 5% CO_2.

Alpha Mouse Liver 12 (AML12) (cat. no. CRL2254; ATCC) cells were cultured in deprivation medium–Ham's F-12 (Gibco – Termofisher Scientific) supplemented with 10% FBS (Invitrogen), 5 g/mL insulin (Thermofisher Scientific), 5 g/mL transferrin (SigmaAldrich), 5 ng/mL selenium (SigmaAldrich), 1% glutamine (Gibco-Life Technologies), and 1% penicillin-streptomycin (Gibco-Life technologies). The cells were plated in 12-well plates at a density of 200,000 cells/mL. AML12 cells were transfected with siRNA (see supplementary material and methods) using Dharmafect-1 (Horizon) according to the manufacturer's instructions. 48h after siRNA transfection, AML12 cells were incubated in DMEM (Gibco – Termofisher Scientific) containing 1 mM glucose, 0.1% fatty acid free BSA (SKU 08810681, MPBio) and supplemented with 10 µM forskolin (FSK) (SigmaAldrich) for 8h.

Immortalized Human Hepatocyte (IHH) (43) cells were cultured in Williams E medium (Invitrogen, CergyPontoise, France) containing 11 mM glucose and supplemented with 10% FBS (Invitrogen), 100 U/mL penicillin, 100 µg/mL streptomycin, 20 mU/mL bovine insulin (SigmaAldrich) and 50 nM dexamethasone (Sigma-Aldrich) (These conditions were stated as "feeding" or "FED"). The cells were plated in 12-well plates at a density of 250,000 cells/mL. IHH cells were transfected with siRNA (see supplementary material and methods) using the Dharmafect1 reagent according to the manufacturer's instructions. After 48h of siRNA transfection, IHH cells were incubated in DMEM (11966025, Gibco) containing 1 mM glucose, 0,1% fatty acid free BSA (SKU 08810681,

MPBio) and supplemented with 10 µM FSK for 8h, referenced as "fasting" or "FAST" media.

Human hepatoma cell line HepG2 cells (cat. No. HB-8065; ATCC) were seeded on 24-well plates and starved during 24h for cell cycle synchronization. Starvation medium was replaced by medium supplemented with 2% FCS containing p16-adenovirus (kind gift of Dr. A. Mazo, University of Barcelona, Spain) or empty adenovirus with a MOI of 60. 24h after infection, medium was replaced by fresh medium with 10% FCS. 72h after infection, cells were collected for Bodipy staining or mRNA analysis.

Reverse transcription real time quantitative-PCR analysis

Total RNA was isolated from cells using EXTRACT ALL® (Eurobio). cDNA was generated using the high capacity reverse transcription kit (Applied Biosystems, Life Technologies, USA). Real-time qPCR was performed on a Stratagene Mx3005P system (Agilent Technologies, Santa Clara, USA) using specific primers (see supplementary material and methods). mRNA levels were normalized to cyclophilin A mRNA and fold induction was calculated using the ddCt method.

Protein extraction and Western Blot Analysis

Cells were scraped in protein lysis buffer (50 mM Tris-HCl, pH 8; 137 mM NaCl; 5 mM EDTA; 2 mM EGTA; 1% TritonX100) on ice, transferred to 1.5 mL Eppendorf tubes and rotated for 20 min at 4°C, followed by sonication for 5 min and centrifugation at 13,000 *g* for 10 min at 4°C. The resulting supernatants were stored in aliquots at −20°C until analysis. Cell lysate protein concentrations were determined using a BCA protein assay kit (Pierce). The protein concentration of samples was equalized and cell lysates were mixed with 4X-LDS non-reducing loading buffer (Life Technologies). Samples were heated at 95°C for 5 min before loading and separated on precast 4–12% BisTris polyacrylamide gels (Life Technologies). Proteins were transferred to a nitrocellulose membrane using the iBlot2 Dry Blotting System (Life Technologies). Membranes were then incubated overnight at 4°C with various primary antibodies in blocking buffer containing 5% non-fat milk at the dilution specified by the manufacturers. The following antibodies were used: p16 (BD Biosciences, 554079), CDK4 (Santa Cruz Biotechnology, sc-260), p-Rb (Abcam, ab10921), AMPK (Cell signaling, #2532), p-AMPK T172 (Cell signaling, #2531).

Cell cycle analysis

Cells were washed with PBS, harvested and fixed with cold 100% ethanol for 10 min at 4°C. Cells were again washed with PBS, centrifuged and incubated with a solution of 50 µg/mL propidium iodide (PI) (SigmaAldrich) with 200 µg/mL RNase A (Qiagen) and NucBlue® (Invitrogen) for 30 min at 37°C. Cells were then washed, resuspended in PBS and were analyzed by flow cytometry with BD LSR Fortessa X-20 cell analyzer (BD Biosciences). PI fluorescence was analyzed with blue laser 488 nm and 575 nm emission filter. NucBlue® fluorescence was analyzed with UV laser 355 nm and 496 nm emission filter. Acquisition was performed with FACS DIVA software (BD Biosciences). PI fluorescence was analyzed on live single-cell population. The percentage of cells in each cell cycle phase was analyzed by using the FlowJo™ software algorithm (BD Biosciences).

Immunofluorescence analysis

IHH cells seeded on coverslips were washed with cold PBS and fixed in 4% paraformaldehyde (PFA) for 10 min at 4°C. Cells were permeabilized with 0.2% Triton X-100 (Euromedex) in PBS for 20 min at room temperature and blocked for 30 min using blocking solution (Bovine Serum Albmin (BSA) 1%, 0.2% Triton X-100 in PBS). Cells were then incubated overnight at 4°C with AMPKα1 (Abcam, ab32047) and AMPKα2 (Abcam, ab3760) antibodies in blocking solution before being washed and incubated 1h at room temperature with secondary antibodies coupled to Alexa 594 (Molecular Probes by Life technologies) and incubated for 10 min with Hoechst (Invitrogen). Cells were mounted in fluorescence mounting medium (GBl Labs). Acquisition was performed using an inverted confocal microscope (LSM 710, Zeiss) with a 40x oil-immersion lens (NA 1.3 with an optical resolution of 176 nm). Alexa 594 and NucBlue were imaged using UV, argon 488 nm and 561 nm lasers. Images were processed with Zen software and analyzed with Icy software.

BODIPY 493/503 staining

Cells seeded on coverslips were fixed in 4% PFA for 10 min at 4°C and incubated with Bodipy 493/503 (Molecular Probes) at 200 ng/mL and NucBlue® for 20 min at room temperature. Cells were mounted in fluorescent mounting medium (GBl Labs). Acquisitions were performed using an inverted confocal microscope (LSM 710, Zeiss) with an airyscan detector and 40x oil-immersion lens (NA 1.3 with an optical resolution of 176 nm) and 1.8X digital zoom. Bodipy and NucBlue fluorescence were imaged using argon 488 nm and UV lasers, respectively. Images were processed with Zen and analyzed with Icy programs respectively.

Mitochondrial activity measurement

Fatty Acid Oxidation Test. Fatty acid oxidation was measured essentially as described previously (44). Freshly isolated primary hepatocytes were plated in DMEM-high glucose (25 mM) + 10% FBS for 4-6h and changed to DMEM-low glucose (5 mM) overnight. 24h after isolation, cells were incubated with 500 µM ^{14}C-palmitic acid:BSA complex. After 3-4h, media was transferred to a CO_2 trap and $^{14}CO_2$ was captured in 1 N NaOH in adjacent wells. Captured $^{14}CO_2$ (complete oxidation) and ^{14}C acid soluble metabolites (ASMs, incomplete oxidation) were subjected to scintillation counting.

Seahorse analysis. Measurements of oxygen consumption rate (OCR) were performed using the XF24 apparatus (Seahorse Bioscience, North Billerica, MA). Briefly, cells were plated into XF24 (V7) polystyrene cell culture plates (Seahorse Bioscience, North Billerica). IHH cells were seeded at 70,000/well (XF24 plate). The cells were incubated for 24h and transfected with siRNA for 48h. Sensor cartridges were calibrated prior to each assay. IHH cells were incubated for 1h in complete Seahorse assay medium (10 mM Glucose, 2 mM Glutamine) supplemented or not with 0.5 mM Etomoxir (Eto) in a 37°C/non-CO2 incubator for 60min prior to the start of an assay. All experiments were performed at 37°C. Each measurement cycle consisted of a mixing time of 3 min, a waiting time of 2 min and a data acquisition period of 3 min. OCR data points represent to the average rates during the measurement cycles. Oligomycin, FCCP and Rotenone/Antimycin A were prepared at respectively 2 µM; 1 µM and 0.5 µM concentrations in desired assay medium and adjusted to pH 7.4. A volume of 50 to 60 µL of compound was added to each injection port. In a typical experiment, 3 baseline measurements were taken prior to the addition of any compound, and 3 response measurements were taken after the addition of each compound. OCR were normalized to protein concentration (pmoles/min/µg proteins).

Oroboros analysis. A piece of liver (125 mg) was minced and homogenized using a Dounce homogenizer at 8-10 strokes in MIR05 respiratory buffer (20 mM HEPES, 10 mM KH_2PO_4, 110 mM sucrose, 20 mM taurine, 60 mM K-lactobionate, 0.5 mM EGTA, 3 mM $MgCl_2 \cdot 6H_2O$, 1 g/L BSA (fatty acid free)). Liver homogenates containing mitochondria (50 µL) were introduced into O2K oxygraph chambers (Oroboros Instruments, Innsbruck, Austria) to assess oxygen consumption in presence of the β-oxidation substrate palmitoyl-carnitine (25 µM), malate (2 mM), followed by ADP (0.5 mM) injection. The respiratory control ratio (RCR) was calculated as the ratio of the state 3 to state 2. Finally, cytochrome C (10 µM) was added to the chamber to measure mitochondrial integrity. Citrate synthase (CS) activity was measured on liver homogenates after the Oroboros experiment.

ROS measurement

Total ROS and mitochondrial superoxide generation was determined using the CellROX Deep Red (Invitrogen) and MitoSOX red (Invitrogen) respectively. Briefly, IHH cells were seeded on a 12-well plate and transfected with siRNA-CTR or siRNA-p16. 48 h after transfectection, IHH cells were harvested and resuspended in culture media containing 5 µM of CellROX or MitoSOX and incubating for 20 min at 37ºC in the dark. Cells were then washed, resuspended in PBS and were analyzed by flow cytometry with BD LSR Fortessa X-20 cell analyzer (BD Biosciences). CellROX fluorescence was analyzed with extinction and emission at 640 nm and 665 nm. MitoSOX fluorescence was analyzed with extinction and emission at 510 nm and 580 nm.

HTRF® P-AMPK and total AMPK assays

A piece of liver (~50 mg) was mechanically disrupted with a Polytron in ~500µL of lysis buffer. Homogenates were centrifuged and

supernatant was collected for protein quantification. Samples containing 0.15 mg/mL or 0.5 mg/mL proteins were respectively added into 96-well HTRF plates for P-AMPK and total AMPK analysis, according to manufacturer's instructions (Cisbio).

STATISTICS

All data were expressed as mean ± standard deviation (SD) or standard error of measurement (SEM), as indicated in the figure legends. Student's unpaired t test was used for assessing statistical differences between two groups, whereas comparison more than two groups was performed using one-way ANOVA. Differences between two groups under two different factors were examined by a two-way ANOVA. In all analyses, a p value of $p < 0.05$ was considered significant.

DATA AND CODE AVAILABILITY

Raw datasets for mouse primary hepatocytes transcriptomics have been deposited in the GEO database through GEO Series accession number GSE134625 (https://www.ncbi.nlm.nih.gov/geo/query/acc.cgi?acc=GSE134625).

ACKNOWLEDGMENTS

This work was supported in part by grants from ANR and European Union: EGID ANR-10-LABX-46 (to BS), PreciNASH ANR-16-RHUS-0006 (to FP, JTH and BS), the Société Francophone de Diabète-SFD (to JTH), the Société Française d'Hépatologie-AFEF (to JTH), and the Contrat Plan État-Région Hauts-de-France - Centre Transdisciplinaire de la Recherche sur la Longévité (CPER-CTRL) grant (to RP and AC). We thank CPER-Région Hauts-de-France for the O2K Oroboros oxygraph. YD was supported by fellowships from INSERM/Région Hauts-de-France, the Nouvelle Société Française d'Atherosclèrose and EGID. JTH was supported by an EMBO Long Term Fellowship (ALTF-277). BS is a recipient of a European Research Council (ERC) Advanced grant (number 694717).

CONFLICT OF INTEREST

The authors declare that they have no conflicts of interest with the contents of this article.

AUTHOR CONTRIBUTION

Y.D., J.T.H., A.K.C., S.A.H. and L.B. performed the experiments. S.C., N.H., E.V., E.D. and K.B.B. contributed to the in vivo experiments. J.T.H., V.L., B.D., P.L. performed microarray analysis. S.L. and J.S.A. advised on mitochondrial function assays, N.M., A.P. and C.A. advised on p16-related assays and cell cycle assays, V.R. and F.P. managed the human cohort. Y.D., J.T.H., A.K.C., and R.P. wrote the manuscript. B.S., J.T.H. and R.P. supervised the study.

REFERENCES

1. LaPak KM, Burd CE. The Molecular Balancing Act of p16INK4a in Cancer and Aging. Mol Cancer Res MCR. 2014 Feb;12(2):167–83.
2. Salazar-Roa M, Malumbres M. Fueling the Cell Division Cycle. Trends Cell Biol. 2017;27(1):69–81.
3. Aguilar V, Fajas L. Cycling through metabolism. EMBO Mol Med. 2010 Sep;2(9):338–48.
4. Sharpless NE, Ramsey MR, Balasubramanian P, Castrillon DH, DePinho RA. The differential impact of p16 INK4a or p19 ARF deficiency on cell growth and tumorigenesis. Oncogene. 2004 Jan;23(2):379–85.
5. Hannou SA, Wouters K, Paumelle R, Staels B. Functional genomics of the CDKN2A/B locus in cardiovascular and metabolic disease: what have we learned from GWASs? Trends Endocrinol Metab TEM. 2015 Apr;26(4):176–84.
6. Bantubungi K, Hannou S-A, Caron-Houde S, Vallez E, Baron M, Lucas A, et al. Cdkn2a/p16Ink4a regulates fasting-induced hepatic gluconeogenesis through the PKA-CREB-PGC1α pathway. Diabetes. 2014 Oct;63(10):3199–209.
7. Denechaud P-D, Lopez-Mejia IC, Giralt A, Lai Q, Blanchet E, Delacuisine B, et al. E2F1 mediates sustained lipogenesis and contributes to hepatic steatosis. J Clin Invest. 2016 Jan;126(1):137–50.
8. Jin J, Valanejad L, Nguyen TP, Lewis K, Wright M, Cast A, et al. Activation of CDK4 Triggers Development of Non-alcoholic Fatty Liver Disease. Cell Rep. 2016 19;16(3):744–56.
9. Ogrodnik M, Miwa S, Tchkonia T, Tiniakos D, Wilson CL, Lahat A, et al. Cellular senescence drives age-dependent hepatic steatosis. Nat Commun. 2017 Jun 13;8(1):15691.
10. Zhang X, Xu GB, Zhou D, Pan Y-X. High-fat diet modifies expression of hepatic cellular senescence gene p16(INK4a) through chromatin modifications in adult male rats. Genes Nutr. 2018 Mar 14;13(1):6.
11. Foretz M, Even PC, Viollet B. AMPK Activation Reduces Hepatic Lipid Content by Increasing Fat Oxidation In Vivo. Int J Mol Sci. 2018 Sep;19(9):2826.
12. Lopez-Mejia IC, Lagarrigue S, Giralt A, Martinez-Carreres L, Zanou N, Denechaud P-D, et al. CDK4 Phosphorylates AMPKα2 to Inhibit Its Activity and Repress Fatty Acid Oxidation. Mol Cell. 2017 Oct 19;68(2):336-349.e6.
13. Kamarajugadda S, Becker JR, Hanse EA, Mashek DG, Mashek MT, Hendrickson AM, et al. Cyclin D1 represses peroxisome proliferator-activated receptor alpha and inhibits fatty acid oxidation. Oncotarget. 2016 Jun 24;7(30):47674–86.
14. Puchalska P, Crawford PA. Multi-dimensional roles of ketone bodies in fuel metabolism, signaling, and therapeutics. Cell Metab. 2017 Feb 7;25(2):262–84.
15. McGarry JD, Foster DW. The regulation of ketogenesis from octanoic acid. The role of the tricarboxylic acid cycle and fatty acid synthesis. J Biol Chem. 1971 Feb 25;246(4):1149–59.
16. Lee Y, Dominy JE, Choi YJ, Jurczak M, Tolliday N, Camporez JP, et al. Cyclin D1-Cdk4 controls glucose metabolism independently of cell cycle progression. Nature. 2014 Jun 26;510(7506):547–51.
17. Coryell PR, Goraya SK, Griffin KA, Redick MA, Sisk SR, Purvis JE. Autophagy regulates the localization and degradation of p16INK4a. Aging Cell. 2020;19(7):e13171.
18. Hinchy EC, Gruszczyk AV, Willows R, Navaratnam N, Hall AR, Bates G, et al. Mitochondria-derived ROS activate AMP-activated protein kinase (AMPK) indirectly. J Biol Chem. 2018 Sep 19;jbc.RA118.002579.
19. Price NL, Gomes AP, Ling AJY, Duarte FV, Martin-Montalvo A, North BJ, et al. SIRT1 is required for AMPK activation and the beneficial effects of resveratrol on mitochondrial function. Cell Metab. 2012 May 2;15(5):675–90.
20. Grabacka M, Pierzchalska M, Dean M, Reiss K. Regulation of Ketone Body Metabolism and the Role of PPARα. Int J Mol Sci. 2016 Dec 13;17(12).

21. Margerie D, Lefebvre P, Raverdy V, Schwahn U, Ruetten H, Larsen P, et al. Hepatic transcriptomic signatures of statin treatment are associated with impaired glucose homeostasis in severely obese patients. BMC Med Genomics. 2019 Jun 3;12(1):80.
22. Hanse EA, Mashek DG, Becker JR, Solmonson AD, Mullany LK, Mashek MT, et al. Cyclin D1 inhibits hepatic lipogenesis via repression of carbohydrate response element binding protein and hepatocyte nuclear factor 4α. Cell Cycle Georget Tex. 2012 Jul 15;11(14):2681–90.
23. Fu M, Rao M, Bouras T, Wang C, Wu K, Zhang X, et al. Cyclin D1 inhibits peroxisome proliferator-activated receptor gamma-mediated adipogenesis through histone deacetylase recruitment. J Biol Chem. 2005 Apr 29;280(17):16934–41.
24. Purushotham A, Schug TT, Xu Q, Surapureddi S, Guo X, Li X. Hepatocyte-specific deletion of SIRT1 alters fatty acid metabolism and results in hepatic steatosis and inflammation. Cell Metab. 2009 Apr;9(4):327–38.
25. Foretz M, Ancellin N, Andreelli F, Saintillan Y, Grondin P, Kahn A, et al. Short-term overexpression of a constitutively active form of AMP-activated protein kinase in the liver leads to mild hypoglycemia and fatty liver. Diabetes. 2005 May;54(5):1331–9.
26. Salt IP, Johnson G, Ashcroft SJ, Hardie DG. AMP-activated protein kinase is activated by low glucose in cell lines derived from pancreatic beta cells, and may regulate insulin release. Biochem J. 1998 Nov 1;335(Pt 3):533–9.
27. McGee SL, Howlett KF, Starkie RL, Cameron-Smith D, Kemp BE, Hargreaves M. Exercise increases nuclear AMPK alpha2 in human skeletal muscle. Diabetes. 2003 Apr;52(4):926–8.
28. Ratman D, Mylka V, Bougarne N, Pawlak M, Caron S, Hennuyer N, et al. Chromatin recruitment of activated AMPK drives fasting response genes co-controlled by GR and PPARα. Nucleic Acids Res. 2016 Dec 15;44(22):10539–53.
29. Zmijewski JW, Banerjee S, Bae H, Friggeri A, Lazarowski ER, Abraham E. Exposure to hydrogen peroxide induces oxidation and activation of AMP-activated protein kinase. J Biol Chem. 2010 Oct 22;285(43):33154–64.
30. Shao D, Oka S, Liu T, Zhai P, Ago T, Sciarretta S, et al. A Redox-Dependent Mechanism for Regulation of AMPK Activation by Thioredoxin1 during Energy Starvation. Cell Metab. 2014 Feb 4;19(2):232–45.
31. Ma D, Panda S, Lin JD. Temporal orchestration of circadian autophagy rhythm by C/EBPβ. EMBO J. 2011 Nov 16;30(22):4642–51.
32. Ezaki J, Matsumoto N, Takeda-Ezaki M, Komatsu M, Takahashi K, Hiraoka Y, et al. Liver autophagy contributes to the maintenance of blood glucose and amino acid levels. Autophagy. 2011 Jul;7(7):727–36.
33. Cassidy LD, Young ARJ, Young CNJ, Soilleux EJ, Fielder E, Weigand BM, et al. Temporal inhibition of autophagy reveals segmental reversal of ageing with increased cancer risk. Nat Commun. 2020 Jan 16;11(1):307.
34. Patsouris D, Mandard S, Voshol PJ, Escher P, Tan NS, Havekes LM, et al. PPARα governs glycerol metabolism. J Clin Invest. 2004 Jul 1;114(1):94–103.
35. Huang B, Wu P, Bowker-Kinley MM, Harris RA. Regulation of Pyruvate Dehydrogenase Kinase Expression by Peroxisome Proliferator–Activated Receptor-α Ligands, Glucocorticoids, and Insulin. Diabetes. 2002 Feb 1;51(2):276–83.
36. Cotter DG, Ercal B, d'Avignon DA, Dietzen DJ, Crawford PA. Impairments of hepatic gluconeogenesis and ketogenesis in PPARα-deficient neonatal mice. Am J Physiol Endocrinol Metab. 2014 Jul 15;307(2):E176-185.
37. Grosse L, Wagner N, Emelyanov A, Molina C, Lacas-Gervais S, Wagner K-D, et al. Defined p16High Senescent Cell Types Are Indispensable for Mouse Healthspan. Cell Metab. 2020 Jul 7;32(1):87-99.e6.
38. Omori S, Wang T-W, Johmura Y, Kanai T, Nakano Y, Kido T, et al. Generation of a p16 Reporter Mouse and Its Use to Characterize and Target p16high Cells In Vivo. Cell Metab. 2020 Sep 18;(32):1–15.

39. Carvalho BS, Irizarry RA. A framework for oligonucleotide microarray preprocessing. Bioinforma Oxf Engl. 2010 Oct 1;26(19):2363–7.
40. Phipson B, Lee S, Majewski IJ, Alexander WS, Smyth GK. ROBUST HYPERPARAMETER ESTIMATION PROTECTS AGAINST HYPERVARIABLE GENES AND IMPROVES POWER TO DETECT DIFFERENTIAL EXPRESSION. Ann Appl Stat. 2016 Jun;10(2):946–63.
41. Alexa A, Rahnenführer J, Lengauer T. Improved scoring of functional groups from gene expression data by decorrelating GO graph structure. Bioinforma Oxf Engl. 2006 Jul 1;22(13):1600–7.
42. Yu G, Wang L-G, Han Y, He Q-Y. clusterProfiler: an R package for comparing biological themes among gene clusters. Omics J Integr Biol. 2012 May;16(5):284–7.
43. Schippers IJ, Moshage H, Roelofsen H, Müller M, Heymans HS, Ruiters M, et al. Immortalized human hepatocytes as a tool for the study of hepatocytic (de-)differentiation. Cell Biol Toxicol. 1997 Jul;13(4–5):375–86.
44. Haas JT, Miao J, Chanda D, Wang Y, Zhao E, Haas ME, et al. Hepatic insulin signaling is required for obesity-dependent expression of SREBP-1c mRNA but not for feeding-dependent expression. Cell Metab. 2012 Jun 6;15(6):873–84.

ABBREVIATIONS

AMPKα: AMP-Activated Protein Kinase Alpha
ATP: Adenosine Triphosphate
CDK: Cyclin-Dependent-Kinase
CDKN2A: Cyclin Dependent Kinase Inhibitor 2A
FAO: Fatty Acid Oxidation
GWAS: Genome-Wide Association Studies
LD: Lipid Droplets
NAFLD: Non-Alcoholic Fatty Liver Disease
p16: p16INK4a
PPARα: Peroxisome Proliferator-Activated Receptor Alpha
PRKAA1/2: 5'-AMP-Activated Protein Kinase Catalytic Subunit 1/2
Rb: Retinoblastoma Protein
SNP: Single-Nucleotide Polymorphism
SIRT1: Sirtuin 1
T2D: Type 2 Diabetes

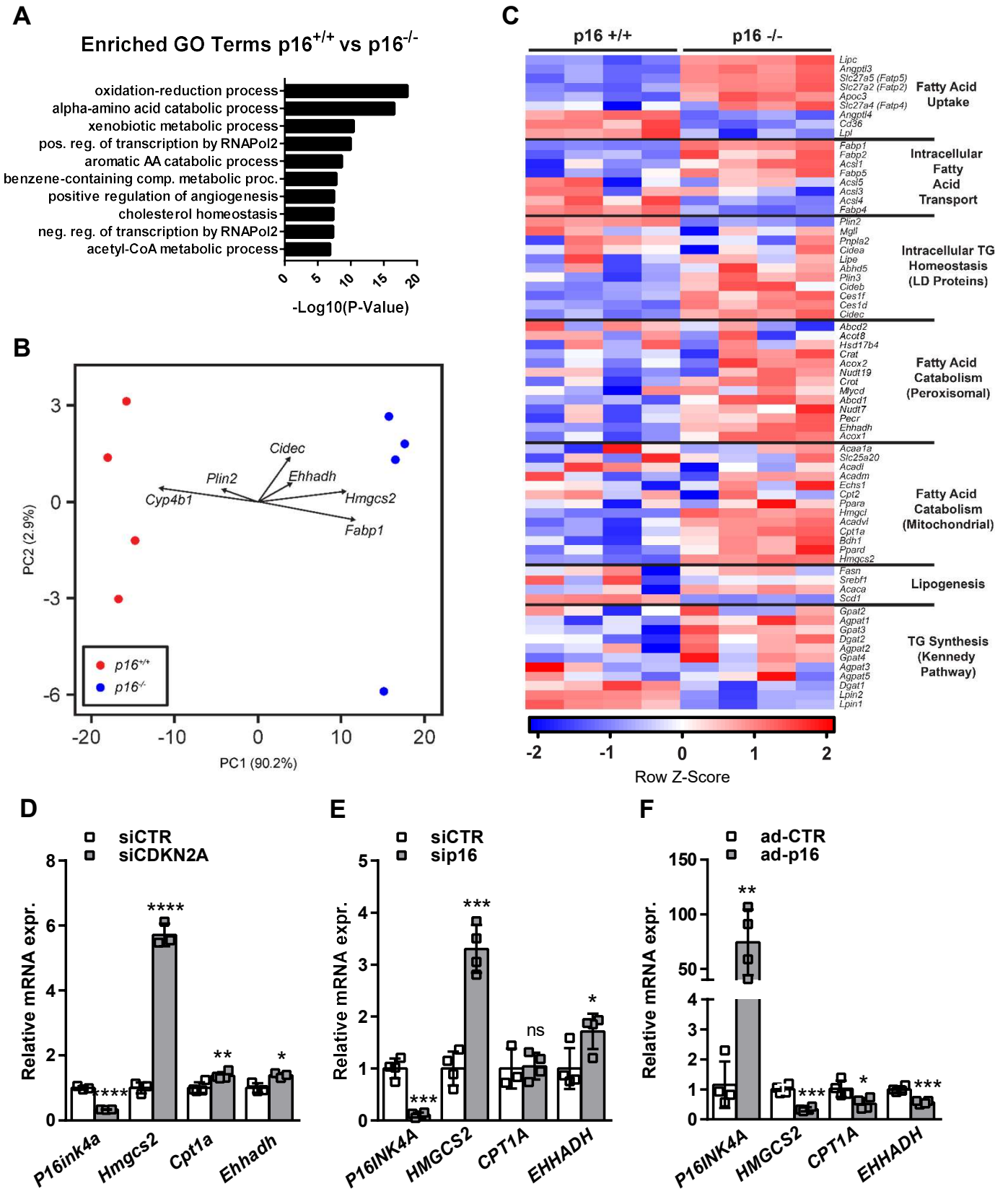

Figure 1. P16-deficiency increases fatty acid catabolism gene expression in hepatocytes. (**A-C**) Primary hepatocytes were isolated from $p16^{+/+}$ and $p16^{-/-}$ mice and incubated for 8 h in 1 mM Glucose DMEM supplemented with 10 µM FSK. (**A**) Gene Ontology terms enrichment for differentially expressed genes between $p16^{+/+}$ and $p16^{-/-}$ primary hepatocytes. (**B**) Principle component analysis of differentially expressed genes between $p16^{+/+}$ and $p16^{-/-}$ primary hepatocytes with selected FAO and ketogenesis gene loadings plotted. (**C**) A heatmap of genes in the major fatty acid metabolic pathways in $p16^{+/+}$ and $p16^{-/-}$ primary hepatocytes. (**D-F**) mRNA relative expression of *P16INK4A*, *HMGCS2*, *CPT1A* and *EHHADH* were measured by QPCR in (**D**) the murine hepatocyte cell line AML12 transfected with siRNA-*CDKN2A* (si*CDKN2A*), (**E**) the human hepatocyte cell line IHH transfected with siRNA-*p16* (si*p16*) and (**F**) the human hepatocyte cell line HepG2 infected with p16-adenovirus (ad-*p16*). All values are expressed as means ± SD. * compared to siCTR or ad-CTR, Unpaired t-test: **** p<0.0001, *** p<0.001, ** p<0.01 and * p<0.05; $$$$ p<0.0001; $$$ p<0.001; $$ p<0.01; $ p<0.05. See also **Figure S1**.

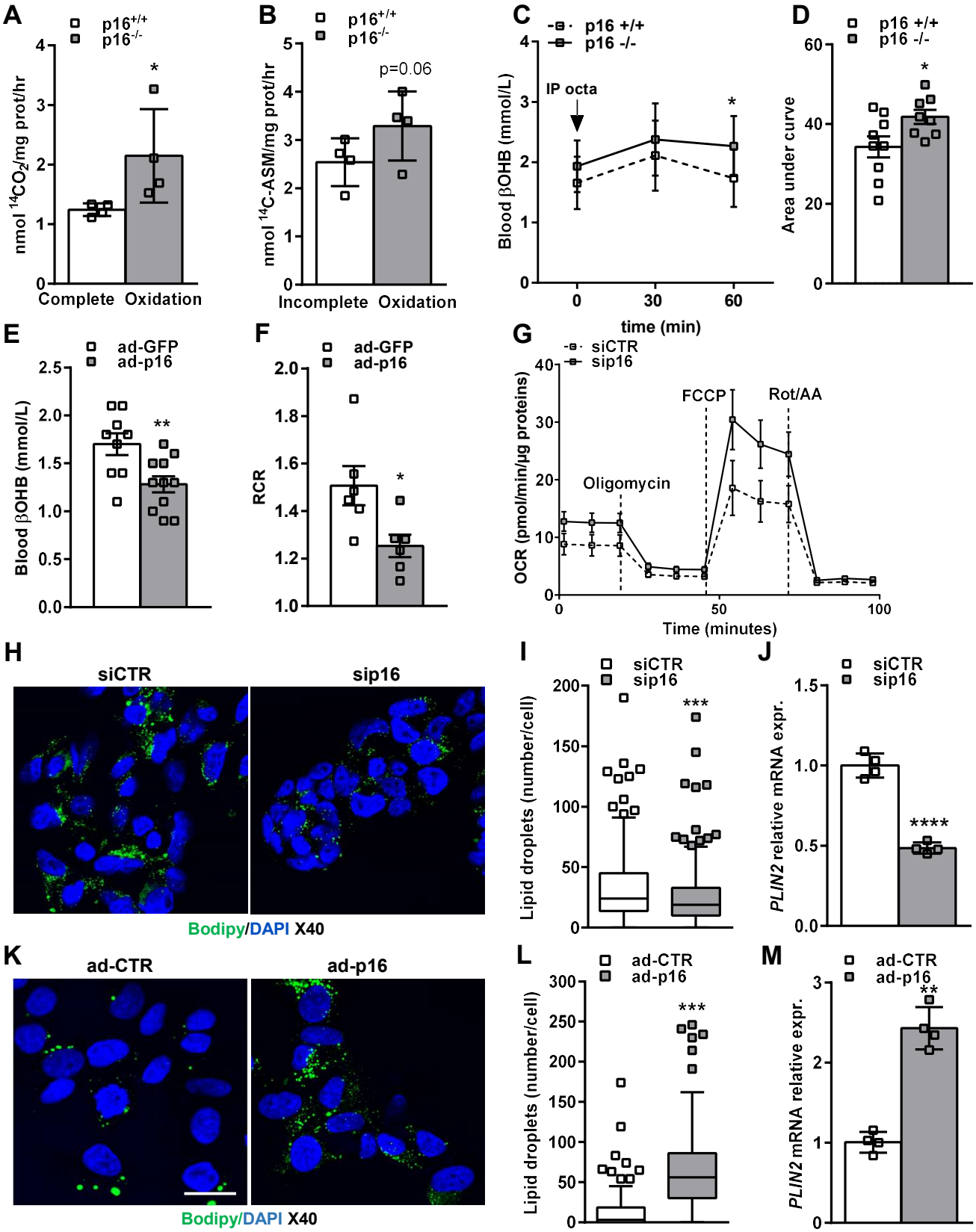

Figure 2. P16 controls mitochondrial fatty acid oxidation and lipid droplet accumulation in hepatocytes. (**A**) complete ($^{14}CO2$) and (**B**) incomplete fatty acid oxidation (^{14}C-ASM) measured in primary hepatocytes isolated from p16$^{+/+}$ and p16$^{-/-}$ mice and incubated with ^{14}C-labeled oleic acid. (**C**) ketone body (β-OHB) production in p16$^{+/+}$ (n=9) and p16$^{-/-}$ (n=9) 12-week-old male mice fasted overnight and injected with a solution of sodium octanoate (250 mM). (**D**) Area under the curve (AUC) of sodium octanoate-stimulated β-OHB production. (**E-F**) 12-week-old male mice were injected with adenovirus GFP (ad-GFP) (n=10) or adenovirus p16 (ad-*p16*) (n=11). (**E**) circulating β-OHB was measured following an overnight fasting. (**F**) Respiratory control ratio (RCR) was measured on liver homogenates from ad-GFP (n=5) and ad-p16 (n=5) injected mice. (**G**) Oxygen Consumption Rate (OCR) in IHH cells transfected with either siCTR or si*p16* for 48 h and incubated for 1 h in Seahorse assay media. Oligomycin: ATP synthase inhibitor. FCCP: mitochondrial uncoupler. Rot/AA: rotenone and Antimycin A, specific inhibitors for ETC complex I and III respectively. (**H**) Representative images of BODIPY 493/503 staining of neutral lipids in IHH cell line transfected with siCTR or si*p16*, Scale bar = 20µm (**I**) Quantification of lipid droplet number per cell with spot tracking plug-in of Icy software. (**J**) *PLIN2* relative mRNA expression in IHH measured by QPCR. (**K-M**) The human hepatocyte cell line HepG2 was infected with an adenovirus expressing the human p16 (ad-*p16*) or a control adenovirus (ad-CTR) for 72 h. (**K**) BODIPY staining of neutral lipids in HepG2 cells. (**L**) quantification of lipid droplets. (**M**) *PLIN2* relative mRNA expression in HepG2 measured by QPCR. All values are expressed as means ± SD (**A, B, G, I, J, L, M**) or means ± SEM (**C, D, E, F**). t test: **** p<0.0001; *** p<0.001; ** p<0.01 and * p<0.05. See also **Figure S2 and S3.**

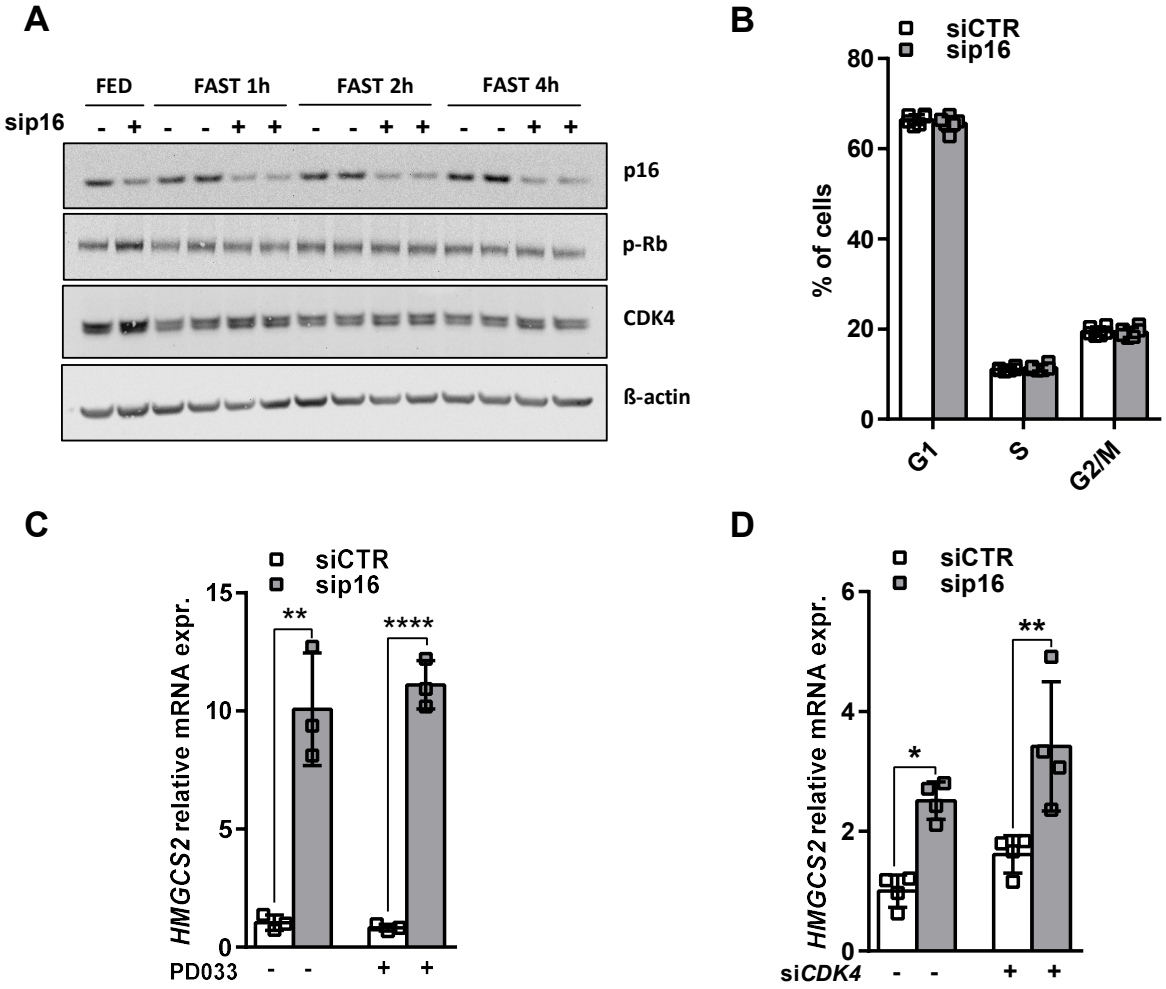

Figure 3. P16 expression modulates *HMGCS2* expression independent of CDK4-Rb-cell cycle control in IHH cells. The human hepatocyte cell line IHH was transfected with either siCTR or si*p16.* (**A**) Western blot of p16, CDK4 and the phosphorylation of Rb in fed condition (FED) and after 1, 2 and 4 h incubation in 1 mM glucose DMEM supplemented with 10 µM FSK (FAST). β-Actin was used as a loading control. (**B**) FACS analysis by propidium iodide staining of the percentage of IHH cells in each phase of the cell cycle after 4 h incubation in 1 mM glucose DMEM supplemented with 10 µM FSK. (**C-D**) Relative *HMGCS2* mRNA expression in IHH cells transfected with siCTR or si*p16* and incubated for 8 h in 1 mM glucose DMEM supplemented with 10µM FSK and (**C**) treated or not with 1 µM of PD0332991 (PD033), the pharmacological inhibitor of CDK4 or (**D**) cotransfected with siRNA-*CDK4* (si*CDK4)* as described in the methods section. All values are expressed as means ± SD. * compared to siCTR of the same condition, one-way ANOVA: **** p<0.0001, ** p<0.01 and * p<0.05. See also **Figure S4.**

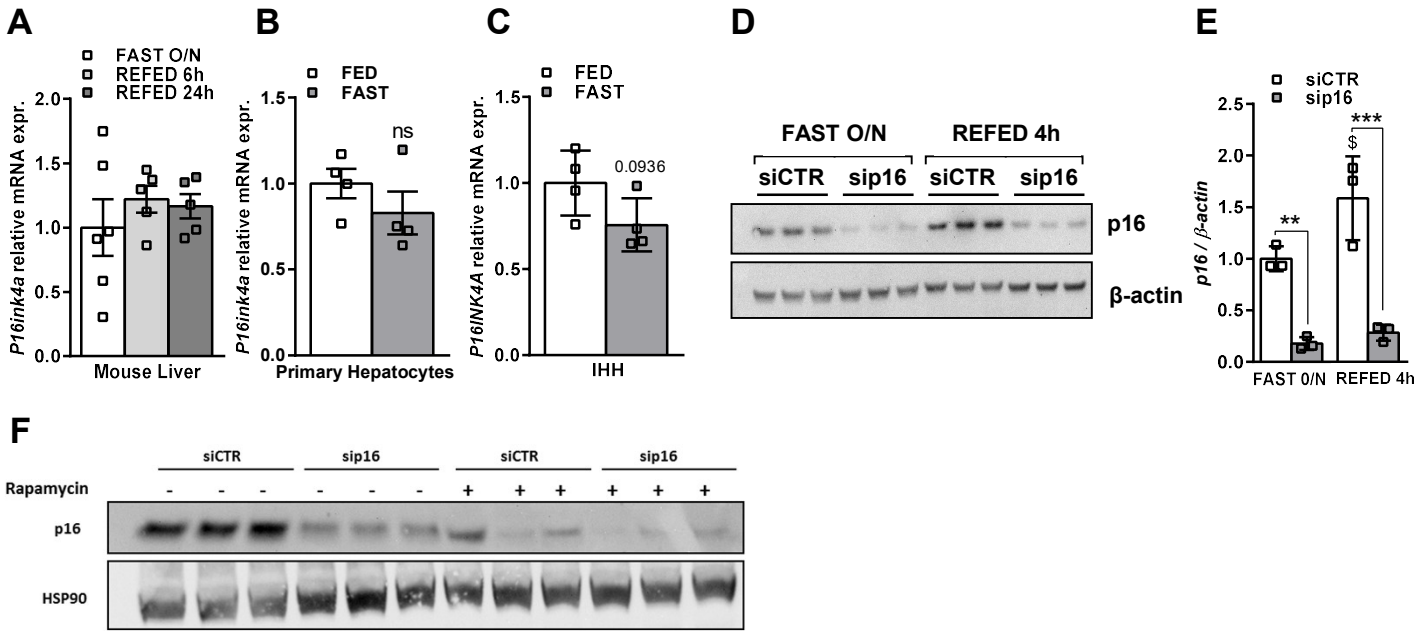

Figure 4. P16 protein expression is modulated by nutritional changes in IHH cells. *P16* mRNA expression was measured by QPCR in **(A)** Liver from mice fasted overnight and refed for either 6h or 24h, **(B)** Primary hepatocytes incubated in media containing 10% serum, 11mM glucose and 100nM insulin (FED) or without serum, 1mM glucose and with glucagon for 8h (FAST), **(C)** IHH hepatocyte cell line incubating in complete media containing serum and insulin (FED) or in fasting media for 8h as described in the methods section. **(D)** p16 protein expression was measured by western blot in IHH cell line transfected with siRNA-CTR or siRNA-p16 and incubating O/N in fasting media and refed for 4h and **(E)** quantification of p16 protein level normalized to β-actin. **(F)** IHH cells were transfected with siRNA-CTR or siRNA-p16 and treated with 100nM Rapamycin or DMSO for 8h in a media containing 10% serum, 11mM glucose and 100nM insulin. p16 protein expression was measured by western blot. All values are expressed as means ± SD (**C, E**) or means ± SEM (**A, B**). * compared to siCTR of the same condition (FAST O/N or REFED4h), one-way ANOVA: *** p<0.001, ** p<0.01 and * p<0.05; $ compared to siCTR or si*p16* in two different conditions (FAST O/N vs REFED 4h) $$$$ p<0.0001; $$$ p<0.001; $$ p<0.01; $ p<0.05.

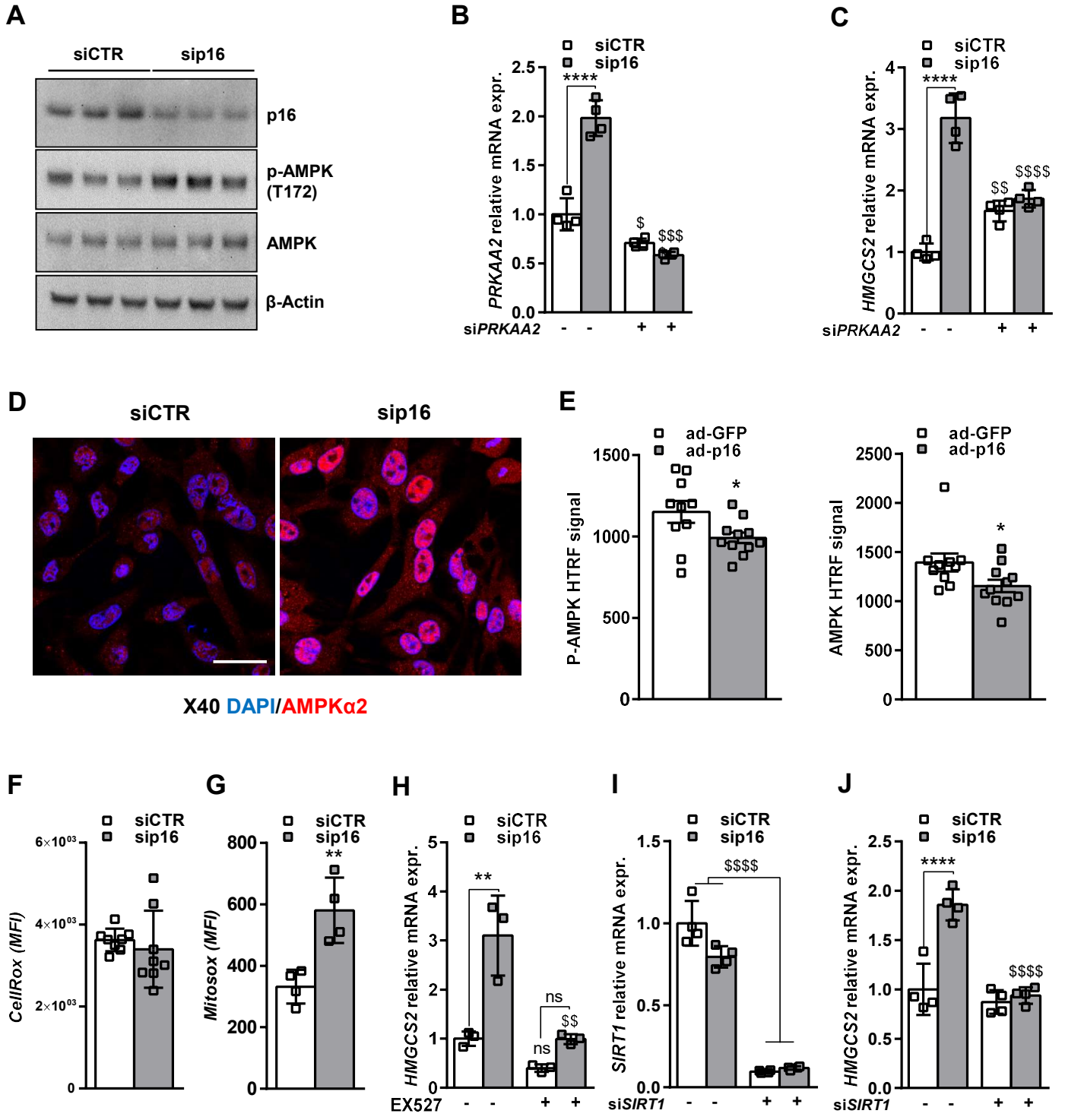

Figure 5. P16 silencing increases *HMGCS2* expression by activating the AMPKα2-SIRT1 pathway. The human hepatocyte cell line IHH was transfected with either siCTR or si*p16* and incubated for 8 h in 1 mM Glucose DMEM supplemented with 10 µM FSK. (**A**) Western blot assay showing protein levels of p16, AMPK and the phosphorylation of AMPK on T172. β-Actin was used as a loading control. (**B**) *PRKAA2* and (**C**) *HMGCS2* relative mRNA expression in IHH cell line cotransfected with si*p16* and siRNA-*PRKAA2* (si*PRKAA2*). (**D**) Representative images of AMPKα2 immunofluorescent staining in IHH cell line transfected with siCTR or si*p16*. Scale bar = 20µm. (**E**) Phospho-AMPK (P-AMPK) and total AMPK signals were analyzed by HTRF technology on liver homogenates from ad-GFP (n=10) or ad-*p16* (n=11) infected mice. (**F**) Total and (**G**) mitochondrial ROS measured respectively by CellROX and MitoROX fluorescent probes in IHH cell line as described in the methods section. (**H**) *HMGCS2* relative mRNA expression in IHH Cell line transfected with siCTR or si*p16* and treated with 10µM EX527. (**I**) *SIRT1* and (**J**) *HMGCS2* relative mRNA expression in IHH cell line cotransfected with si*p16* and siRNA-SIRT1 (si*SIRT1*). All values are expressed as means ± SD (**B, C, F, G, H, I, J**). * compared to siCTR of the same condition (DMSO, treatment or siRNA), one-way ANOVA: **** p<0.0001; *** p<0.001; ** p<0.01 and * p<0.05; $ compared to siCTR or si*p16* in two different conditions (DMSO vs treatment or scramble vs siRNA) $$$$ p<0.0001; $$$ p<0.001; $$ p<0.01; $ p<0.05. All values are expressed as means ± SEM (**E, F**). t test: * p<0.05. See also **Figure S5.**

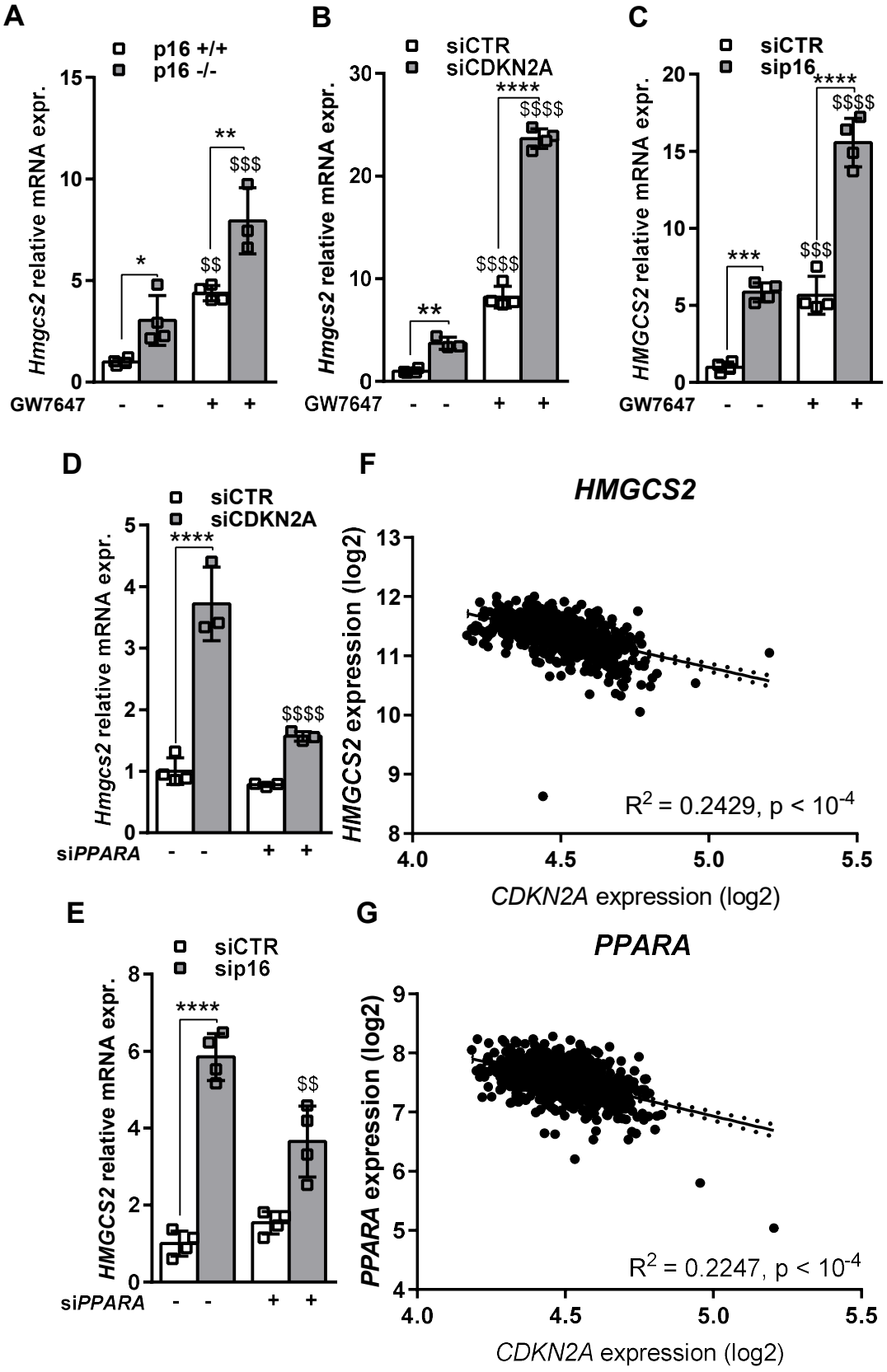

Figure 6. P16-deficiency increases fatty acid catabolism gene expression via activation of PPARα in hepatocytes. (**A-C**) *HMGCS2* relative mRNA expression measured by QPCR in (**A**) primary hepatocytes isolated from $p16^{+/+}$ and $p16^{-/-}$ mice, (**B**) murine AML12 cell line transfected with siRNA-CTR (siCTR) or siRNA-*CDKN2A* (si*CDKN2A*) for 48h, (**C**) human IHH cell line transfected with siCTR or siRNA-*p16* (si*p16*) for 48h and treated with 600 nM GW7647 for 8 h or DMSO. (**D-E**) *HMGCS2* relative mRNA expression measured by QPCR in (**D**) murine AML12 and (**E**) human IHH cell lines transfected respectively with si*CDKN2A* ***or*** si*p16* and cotransfected with siRNA-*PPARA* (si*PPARA*) for 48 h. All values are expressed as means ± SD. * compared to siCTR of the same condition (DMSO, treatment, siCTR or si*PPARA*), one-way ANOVA: *** p<0.001, ** p<0.01 and * p<0.05; $ compared to siCTR or si*p16* in two different conditions (DMSO vs GW7647 or siCTR vs si*PPARA*) $$$$ p<0.0001; $$$ p<0.001; $$ p<0.01; $ p<0.05. (**F-G**) Plots of hepatic CDKN2A expression versus (**F**) *HMGCS2*, (**G**) *PPARA* expression in human liver biopsies obtained during abdominal surgery (n=910 patients) as described in the methods. Values are reported for R^2 as well as the linear regression best fit equation. The best fit line and 95% confidence intervals are plotted on the graphs. See also **Figure S6** and **Table S1.**